DMD Fast Forward. Published on April 8, 2019 as DOI: 10.1124/dmd.118.086090
This article has not been copyedited and formatted. The final version may differ from this version.

Mechanism of Reductive Metabolism and Chiral Inversion of Proton Pump Inhibitors

Chongzhuang Tang[a,b], Zhaoqiang Chen[a,b], Xiaojian Dai[a], Weiliang Zhu[a,b], Dafang Zhong[a,b], Xiaoyan Chen[a,b]

[a] Shanghai Institute of Materia Medica, Chinese Academy of Sciences, 501 Haike Road, Shanghai 201203, P.R. China (C.T., Z.C., X.D., W.Z., D.Z., X.C.)

[b] University of Chinese Academy of Sciences, No.19A Yuquan Road, Beijing 100049, China (C.T., Z.C, W.Z., D.Z., X.C.)

Running title: Mechanism of chiral inversion of proton pump inhibitors

Corresponding author:

Xiaoyan Chen, Ph. D.

Shanghai Institute of Materia Medica, Chinese Academy of Sciences, 501 Haike road, Shanghai 201203, China.

E-mail: xychen@simm.ac.cn

Number of text pages: 23

Number of tables: 4

Number of figures: 8

Number of references: 43

Number of words in Abstract: 247

Number of words in Introduction: 606

Number of words in Discussion: 1262

Abbreviations: ABT, 1-aminobenzotriazole; AUC, area under the plasma concentration-time curve; CYP, cytochrome P450; DMSO, dimethyl sulfoxide; EA, ethacrynic acid; GSH, reduced glutathione; HLMs, human liver microsomes; HLC, human liver cytosolic fractions; LAN, lansoprazole; LC-MS/MS, liquid chromatography-tandem mass spectrometry; MD, menadione; NADH, nicotinamide adenine dinucleotide; NADPH, nicotinamide adenine dinucleotide phosphate; NBO, natural bond orbital; NEM, *N*-ethylmaleimide; OME, omeprazole; PBS, phosphate buffer solution; PPIs, proton pump inhibitors; RAB, rabeprazole; SD rats, Sprague–Dawley rats; UPLC-Q-TOF MS, ultra-high-performance liquid chromatography–quadrupole time-of-flight mass spectrometry.

Abstract

Racemic proton pump inhibitors (PPIs) have been developed into pure enantiomers given superior pharmacokinetic profiles. However, after doses of single enantiomer PPIs, different degrees of chiral inversion were observed. We investigated the relationship between chiral inversion and reductive metabolism of PPIs, as well as the mechanism of reductive metabolism. In liver microsomes and Sprague–Dawley rats, PPI-thioethers were stereoselectively oxidized to (*R*)- and (*S*)-PPIs, indicating that thioethers could be the intermediates of chiral inversion. By comparing the AUC ratios of thioether to rabeprazole under different routes of administration and blood sampling site, it was determined that thioether was mainly formed in the liver rather than the intestine. The formation rate of PPI-thioethers in liver subcellular fractions was significantly higher than that in buffers. Sulfhydryl-blocking agents, such as *N*-ethylmaleimide, menadione, and ethacrynic acid, could inhibit the reductive metabolism of PPIs *in vitro*, and their corresponding glutathione conjugates were observed. Similar amounts of thioethers were formed in glutathione solutions as in liver subcellular fractions, indicating that biological reducing agents, instead of reductases, accelerated the reductive metabolism of PPIs. The reduction rates in glutathione solutions were ordered as follows: rabeprazole > omeprazole > lansoprazole > pantoprazole, which was consistent with the natural bond orbital charges of sulfur atoms in these compounds. In conclusion, PPIs were transformed into thioethers by biological reducing agents in liver, and thioethers continued to be oxidized to two enantiomers, leading to chiral inversion. Furthermore, inhibiting oxidative metabolism of PPIs could enhance reductive metabolism and chiral inversion.

Introduction

Benzimidazole proton pump inhibitors (PPIs) are used for the treatment of acid-related diseases such as gastric ulcers and non-erosive gastroesophageal reflux disease (Freedberg et al., 2017). Their molecular skeletons contain chiral sulfoxide groups. The early marketed PPIs, including omeprazole (OME), lansoprazole (LAN), pantoprazole (PAN), and rabeprazole (RAB), are all racemic mixtures with two enantiomers exhibiting different pharmacokinetic and/or pharmacodynamic properties (Freedberg et al., 2017). For example, (*R*)-OME and (*R*)-PAN show extensive variability in pharmacokinetics in humans due to CYP2C19 genetic polymorphism, but the metabolic clearance of (*S*)-OME and (*S*)-PAN is independent of CYP2C19 (Ishizaki and Horai, 1999; Horn, 2004). Researchers have gradually realized the therapeutic advantages of single enantiomer forms of PPIs, including reducing the metabolic load on the body, simplifying pharmacokinetics, providing benefit to non-responders to standard dose of racemate, more homogenous response to treatment, and better efficacy with equal safety (Zhou et al., 2008). Developing single enantiomer PPIs has become a trend (Agranat et al., 2002). (*S*)-OME, (*R*)-LAN, (*S*)-PAN, and (*R*)-RAB have already been marketed in different countries (Shin and Kim, 2013).

For single enantiomer drugs, good in vitro and in vivo chiral stability is required (Williams et al., 1998). The US Food and Drug Administration states that if a racemate has been marketed and the sponsor wishes to develop the single enantiomer, evaluation should include determination of whether there is significant conversion to the other isomer (Tomaszewski and Rumore, 1994). If the pure enantiomer is chirally unstable, readily converting to a mixture of two enantiomers, then the stereoselective synthesis, chiral separation, and quality control would be in vain. Single enantiomers may undergo enzymatic or nonenzymatic chiral inversion. For example, 2-arylpropionic acid

undergoes unidirectional chiral inversion of the inactive (*R*)-enantiomer to the active (*S*)-enantiomer (Ikuta et al., 2017). Thalidomide was marketed in racemic form to treat morning sickness in pregnant women, and strong embryotoxicity and teratogenicity of (*S*)-thalidomide were found. (*R*)-enantiomer was considered to be brought on to the market at one point in time, but subsequent studies have proved that the chiral center in thalidomide was unstable in protonated media and underwent a rapid chiral inversion. Therefore, (*R*)-thalidomide could still cause toxic reactions due to in vivo chiral inversion (Reist et al., 1998).

Cases of chiral inversion of single enantiomer PPIs in clinical pharmacokinetic studies have been reported (Andersson et al., 2001; Xie et al., 2004). After an oral administration of 40 mg (*S*)-OME, the chiral inversion based on plasma exposure (AUC_R/AUC_S) reached 0.4% in humans. After an oral administration of (*R*)-PAN, the average $AUC_{0\text{-}t}$ of (*S*)-PAN accounted for 1.5% of the total PAN. A phase I clinical trial in our laboratory found that after a single oral dose of 80 mg of (*R*)-anaprazole, the chiral inversion ratio reached 6.3% ± 5.7% (data not yet published). To date, the mechanism of chiral inversion in vivo and the reasons for the differences in chiral inversion of PPIs have not been reported.

The chemical racemization of sulfoxides occurred at approximately 200°C through a pyramidal inversion (Rayner et al., 1968; Marom et al., 2007); therefore, the sulfoxide groups were considered chirally stable in vivo. We speculated that the chiral inversion of PPIs was related to their metabolic transformation. Oxidative metabolism and reductive metabolism of PPIs could both occur in vivo to form sulfone and thioether, respectively. According to our early results, PPI sulfone could not be re-metabolized to sulfoxide, whereas thioethers could be easily oxidized to sulfoxides. Consequently, a hypothesis was proposed that thioether metabolites of PPIs were the intermediate of

DMD Fast Forward. Published on April 8, 2019 as DOI: 10.1124/dmd.118.086090
This article has not been copyedited and formatted. The final version may differ from this version.

chiral inversion.

In this study, we investigated the relationship between chiral inversion and reductive metabolism of PPIs, as well as the mechanism of reductive metabolism.

Materials and methods

Chemicals and reagents. Pooled human liver microsomes (HLMs), human liver cytosolic fractions (HLCs), recombinant flavin-containing monooxygenases (FMOs), including FMO1, FMO3, and FMO5 were supplied by BD Gentest (Woburn, MA, USA). Fresh rat liver homogenate and rat liver S9 were prepared according to the reported methods (Esterbauer et al., 1985; Bourland et al., 1998). (*R*)- and (*S*)-LAN, (*S*)-OME, and (*R*)-PAN were purchased from TRC Chemicals (Toronto, Canada). (*S*)-PAN was bought from Sun-Wise Pharmaceutical (Hefei, China). (*R*)-OME was purchased from Santa Cruz Biotechnology (Santa Cruz, CA). (*R*)- and (*S*)-RAB were kindly provided by Aosaikang Pharmaceutical (Jiangsu, China). The racemic forms of OME, LAN, PAN, and RAB and their thioether metabolites, (*R*)-LAN-d4, 1-aminobenzotriazole (ABT), reduced glutathione (GSH), nicotinamide adenine dinucleotide phosphate (NADPH), nicotinamide adenine dinucleotide (NADH), ethacrynic acid (EA), menadione (MD), *N*-ethylmaleimide (NEM), cysteine, and dimethyl sulfoxide (DMSO), were purchased from Meilunbio (Dalian, China).

Animal experiments. All procedures in animal studies were performed in accordance with the *Guide for the Care and Use of Laboratory Animals* of Shanghai Institute of Materia Medica, Chinese Academy of Sciences. Male Sprague–Dawley (SD) rats weighing 180–220 g were acclimatized for at least 7 days. The portal vein-cannulated male SD rats were purchased from Vital River Laboratory Animal Technology Co., Ltd (Beijing, China). Animals were fasted for 12 h with free access to water before the experiments. Blood samples were collected pre-dosage (0 h) and 0.083, 0.25, 0.5, 1, 1.5, 2, 3 and 4 h post-dosage in tubes containing heparin, and additional two blood samples at 6 h and 8 h post-dosage were also collected in the experiment–"Effect of inhibiting CYP enzymes on the chiral inversion". Plasma was acquired after

centrifugation of blood samples at 14,000 rpm for 5 minutes. The isolated plasma samples (50 μL) were placed in covered storage tubes containing 1% diethylamine solution (2 μL) as a stabilizer (Uno et al., 2005) and stored at −80°C until analysis.

Biotransformation of RAB thioether in SD rats. RAB thioether was dissolved in DMSO and then diluted to 200 μg/mL with normal saline. The final concentration of DMSO was 1%. RAB thioether was administered intravenously via the tail vein to five male SD rats at a dose of 1 mg/kg. Plasma samples were collected, prepared, and stored as mentioned above.

Pharmacokinetic study of (*R*)-RAB in SD rats via various routes of administration and blood sampling site. This experiment aimed to determine whether the intestine was the main site of PPIs reductive metabolism. The portal vein-cannulated SD rats (n = 5) were orally administered with 3 mg/kg (*R*)-RAB. The normal male SD rats were divided into two groups (n = 4 in each) and were administered with the same dose of (*R*)-RAB via intravenous and portal vein administration respectively. Rats in the portal vein administration group were anaesthetized by intraperitoneal injection of nembutal (30 mg/kg); then, the hepatic portal vein was exposed by abdominal incision for administration. (*R*)-RAB was dissolved in sodium bicarbonate buffer (pH 10). In the portal vein-cannulated rats, blood samples were taken from portal vein and the retro-orbital venous plexus at the same time. In other two groups, blood samples were collected only from the retro-orbital venous plexus.

Effect of inhibiting CYP enzymes on the chiral inversion. Rats were divided into the ABT group (n = 4) and control group (n = 4). In the ABT group, rats were orally administered with 100 mg/kg of ABT 16 h prior to the experiment, and the rats in the control group were given the same volume of normal saline. Then, rats were intravenously injected with 3 mg/kg of (*R*)-RAB. Plasma samples were collected,

stored, and prepared as mentioned above.

Incubation of RAB in liver subcellular fractions. RAB was dissolved in DMSO to obtain stock solutions (100 mM), which were then diluted with phosphate buffer solution (PBS) to the desired concentration, and the final system contained a DMSO concentration of 0.1% (v/v). RAB (1.5 μM) was incubated in several kinds of liver subcellular components (HLMs, HLCs, heated HLCs, freshly prepared rat liver homogenate, and acetonitrile extract of freshly prepared rat liver homogenates (5:1, v/v)) at 37°C for 1 h. Reduced coenzymes such as NADPH (1 mM) and NADH (0.1 mM) were added to HLC incubations respectively to evaluate whether reductases were involved in the reductive metabolism. (*R*)-RAB (10 μM) was also incubated in rat liver S9 (1mg/mL) in the absence (-) and presence (+) of NADPH (1 mM) or GSH (1 mM), either individually or in combination. After incubation, 100 μL of ice-cold acetonitrile containing 0.1% diethylamine was added to terminate the reaction, and the mixture was stored at −80°C until the analysis of RAB thioether. Results are presented as means ± standard deviation (S.D.) from three triplicate experiments. The main metabolites in rat liver S9 incubations were detected using UPLC-Q-TOF MS.

Inhibition of the reductive metabolism of RAB. HLCs were pre-incubated with different concentrations (25, 100, and 1000 μM) of sulfhydryl-blocking agents, such as NEM, EA, and MD, for 15 minutes. Then, RAB was added to initiate the reaction. After 1 h incubation, ice-cold acetonitrile containing 0.1% diethylamine was added to terminate the reaction and stored at −80°C until the analysis of RAB thioether.

Incubations of PPIs in GSH and cysteine solutions. Four PPIs were incubated with GSH to confirm whether the thiol-containing molecules in liver subcellular fractions could accelerate the reduction of PPIs and evaluate the effect of thiol concentration on the reduction of PPIs. GSH and cysteine were prepared in deionized water to obtain 10

mM stock solutions, which was then gradually diluted to different concentrations (5, 10, 25, 50, 100, 500, and 1000 μM) with PBS or KPi (a stronger capacity buffer to avoid the change in acidity due to increased GSH or cysteine concentration). RAB (1.5 μM) were incubated with GSH or cysteine solutions for 1 h at 37°C. After incubation, the reaction was stopped with cold acetonitrile solution containing 1 mM NEM. Equal concentrations of OME, LAN, PAN, and RAB (1.5 μM) were incubated with HLCs (1 mg/mL) and GSH (1000 μM) under the same conditions, respectively. At predetermined time intervals (0, 5, 15, 30, and 60 minutes), ice-cold acetonitrile containing 1 mM NEM was added to terminate the reactions. All terminated samples were stored at −80°C until the quantitative determination of thioether metabolites by liquid chromatography tandem-mass spectrometry (LC-MS/MS).

Incubation of PPI-thioethers in HLMs and FMOs. The conditions for incubation in HLMs were optimized to be linear with respect to incubation time and protein concentrations. The final incubation mixture contained substrate, HLMs (0.1 mg/mL), and NADPH (1 mM) in a final volume of 200 μL of 100 mM PBS (pH 7.4). The mixtures were preincubated for 5 minutes at 37°C, and each reaction was initiated by adding various concentrations of PPI-thioethers (0.4, 2, 4, 8, 16, 32, 48, 80, and 200 μM). The control HLM was heat inactivated at 45°C for 2 min wherein the FMO activity was abolished but not the CYPs. After incubation at 37°C for 10 minutes, 400 μL of acetonitrile containing 0.1% diethylamine and an internal standard (200 ng/mL (*R*)-LAN-d4) was added to terminate the reaction. The mixtures were vortexed for 1 minutes and centrifuged at 13,000 g at 4°C for 5 minutes. A 100 μL aliquot of the supernatant was diluted 10-fold with the mobile phase, and then 5 μL of the resulting solution was injected into the LC-MS/MS system to determine the concentrations of (*R*)- and (*S*)-PPIs. Experiments were performed in duplicate. Incubations of PPI-

thioethers were also conducted in recombinant FMOs. The PPI-thioethers were added at a final concentration of 3 μM (DMSO 0.1%) to a final volume of 100 μl of PBS (100 mM, pH 7.4). A stock solution of FMOs (FMO1, FMO3, and FMO5) or HLM were also added at final concentrations of 1.0 mg/mL. The mixtures were preincubated at 37°C for 3 minutes, and the reactions were initiated by the addition of NADPH at a final protein concentration of 1 mM. The mixtures were incubated at 37°C for 60 minutes, quenched by the addition of an equal volume of acetonitrile containing 0.1 % diethylamine. All terminated samples were stored at −80°C until the quantitative determination of (*R*)- and (*S*)-PPIs by chiral LC-MS/MS.

Sample preparation. (*R*)-LAN-d4 (25 μL) in methanol (200 ng/mL) was added as an internal standard to mixtures of 25 μL of plasma samples or incubation samples and 200 μL of acetonitrile containing 0.1% diethylamine. The mixtures were vortexed for 1 minutes and centrifuged at 13,000 g at 4°C for 5 minutes. Then, 1 μL of the supernatant was injected into the LC-MS/MS system.

Determination of PPI-enantiomers and thioether metabolites in plasma samples or incubation samples by chiral LC-MS/MS. The HPLC system consisted of a LC-30AD pump equipped with a SIL-30AC autosampler (Shimadzu, Kyoto, Japan). Chiral separation of PPI-enantiomers was performed on Lux Cellulose-4 chiral columns (150 × 4.6 mm, 5 μM) from Phenomenex (Torrance, CA, USA) at 40°C with a flow rate of 0.8 mL/min. The separation was carried out with gradient elution procedure. Mobile phase A (5 mM ammonium acetate) and B (acetonitrile/isopropanol (30:70, v/v)) ratios linearly changed as follows: 0–0.8 min, 25% B; 0.8–2.1 min, 25%–43% B; 2.1–3.6 min, 43%–55% B; 3.6–4.6 min, 55%–95% B; 4.6–4.8 min, 95% B. Then, the column was equilibrated with the initial mobile phase. When analyzing PAN enantiomers, the gradient elution procedure was slightly modified to obtain a better resolution. The total

run time was 6.5 min.

MS detection was performed using an AB Sciex Triple Quad 6500 System (Applied Biosystems, Concord, ON, Canada) equipped with a TurboIonSpray ion source. Multiple reaction monitoring was used to quantify compounds in the positive ion mode (*m*/z 330.1 → *m*/*z* 182.1 for OME thioether, *m*/*z* 346.1 → *m*/*z* 198.1 for OME, *m*/z 354.2 → *m*/*z* 236.2 for LAN thioether, *m*/z 370.2 → *m*/*z* 252.2 for LAN, *m*/z 368.2 → *m*/*z* 184.2 for PAN thioether, *m*/z 384.2 → *m*/*z* 200.2 for PAN, *m*/z 344.2 → *m*/*z* 226.2 for RAB thioether, and *m*/z 360.2 → *m*/*z* 242.2 for RAB).

Sample preparation and ultra-high-performance liquid chromatography–quadrupole time-of-flight mass spectrometry (UPLC-Q-TOF MS) analysis. The reductive metabolism of PPIs in HLCs was significantly inhibited by sulfhydryl-blocking agents (NEM, EA, and MD). Supposedly, certain reductive agents were depleted by these compounds. Acetonitrile (800 μL) was added to a 200 μL aliquot of the HLC incubations that were treated with NEM, EA, or MD and GSH incubations. These samples were vortex-mixed and centrifuged at 14,000 g for 5 minutes. The supernatant was transferred into a plastic tube, evaporated to dryness under a stream of nitrogen at 40°C, and then reconstituted in 120 μL of water/methanol (98:2, v/v) solution. A 7 μL aliquot of the reconstituted solution was injected into the UPLC-Q-TOF Synapt G2 (Waters, Milford, MA, USA) system for analysis. The rat liver S9 incubations were prepared as described above except that the reconstitution reagent was replaced with acetonitrile containing 0.1% diethylamine as a stabilizer.

The analytes in GSH incubations and inhibitor-treated HLC incubations were separated with a mobile phase consisting of deionized water containing 0.1% formic acid as the aqueous phase and methanol as the organic phase by using an Acquity HSS T_3 column (100 × 2.1 mm, 1.8 μM) equilibrated at 40°C. The column was eluted with

a linear gradient of 2%–50% B over initial time to 6.0 min, 50%–70% B over 2.0–7.0 min, 70%–99% B over 7.0–11.0 min and held at 99% B for 1.0 min, returned to 1% B for 0.5 min, and then held for 1.5 min at an eluent flow rate of 0.40 mL/min. The chromatographic separation of analyte in rat liver S9 incubations was conducted using Lux Cellulose-4 chiral columns (150 × 4.6 mm, 5 μM) from Phenomenex (Torrance, CA, USA) at 40°C with a flow rate of 0.8 mL/min. The mobile phase was a mixture of 5 mM ammonium acetate (A) and acetonitrile/isopropanol (30: 70, v/v) (B). The gradient was started from 30% B and maintained for 3 min and increased linearly to 50% B in the next 11 min. Afterward, the gradient was rapidly increased to 99% B and maintained for 1 min, reduced to 30% B for 1 min, and finally, maintained at 30 % B for 2.5 min to equilibrate the column. For Q-TOF MS analysis, the optimal conditions were as follows: capillary voltage of 3000 V, desolvation temperature of 450°C, sample cone voltage of 35 V, source temperature of 120°C, cone gas flow of 50 L/h, and desolvation gas flow of 800 L/h. The mass spectrometric MS^E data were acquired in the positive ion mode from 50 Da to 1200 Da with a 0.15 s scan time at a constant collision energy setting of 2 V during low-energy MS mode (function 1) for precursor ion data and then dynamically from 15 V to 40 V collision energy during the high-energy MS^E mode (function 2) for optimal fragmentation data. Mass was corrected during acquisition using an external reference (LockSpray™) consisting of a 40 ng/mL solution of leucine enkephalin infused at a flow rate of 10 μL/min via a LockSpray interface, generating a reference ion for positive ion mode ($[M+H]^+$ = 556.2771) to ensure accuracy during the MS analysis.

Data analysis. WinNonlin (version 6.1, Pharsight Corp., Cary, NC, USA) was used to calculate the pharmacokinetic parameters in a non-compartmental model. GraphPad Prism (version 5.0, GraphPad Software Inc., San Diego, CA, USA) was used to

generate the K_m and V_{max} values. All data were expressed as mean ± S.D.

Results

Stereoselective oxidation of RAB thioether in SD rats. To test whether RAB thioether could be oxidized to parent drug, rats were administered intravenously with 1 mg/kg RAB thioether. The average concentration versus time profiles are shown in Fig. 1. (*R*)- and (*S*)-RAB were observed in rat plasma from the first blood sampling time. RAB thioether and RAB enantiomers were all eliminated rapidly from plasma. The biotransformation of RAB thioether to (*R*)- and (*S*)-enantiomers was stereoselective. Plasma concentration of (*R*)-RAB was significantly higher than that of (*S*)-RAB.

Stereoselective oxidation of PPI-thioethers in HLMs and FMOs. Thioether metabolites of OME, LAN, PAN, and RAB were incubated with HLMs, and the concentrations of the corresponding (*R*)- and (*S*)-enantiomers were determined by LC-MS/MS. Nonlinear regression analysis was used to calculate the kinetic parameters (K_m and V_{max}) as shown in Table 1. The oxidative metabolism of PPI-thioethers to form sulfoxides were all stereoselective. In addition to PAN thioether, three other PPI-thioethers were preferentially metabolized to their (*R*)-enantiomers. (*R*)- and (*S*)-PPIs were also detected in thioether-fortified incubated samples with FMO1, FMO3, and FMO5, but the yields were significantly lower than those in HLM incubations (Supplemental Fig. 1). And the formation in FMO-deactivated liver microsomes (by heating) showed no difference with that in the untreated liver microsomes. Therefore, CYPs were considered as the main enzymes involved in the oxidation of thioethers to PPIs .

Formation region of RAB thioether in vivo. After administration of (*R*)-RAB to rats via different routes, the area under the plasma concentration–time curve (AUC) data of

the parent drug and RAB thioether are shown in Table 2. Following oral administration, the concentrations of RAB and RAB thioether in portal vein were both higher than that in systemic circulation, however, the molar AUC_{0-t} ratios of thioether to RAB in the portal vein was significantly lower than that in the systemic circulation (11.8% versus 30.6%). The molar AUC_{0-t} ratios were 15.5% and 28.6% in rats administered via intravenous and portal vein routes, respectively. These data indicated that RAB thioether was mainly formed in the liver instead of the intestine.

Metabolism of (*R*)-RAB in liver subcellular fractions. To elucidate the formation pathway of RAB thioether, (*R*)-RAB was incubated with liver subcellular fractions and PBS. The amount of produced RAB thioether is shown in Fig. 2. After 1 h incubation, approximately 13.3% of RAB was transformed into thioether in HLCs, a similar amount of thioether was formed in RLH, and a slightly lower amount was found in HLMs. However, only 2.35% was found in PBS. The formation of thioether was not increased with the addition of NADPH or NADH to HLC incubations. Heat-deactivated HLCs (HLCs were heated for 10 minutes in a 100°C water bath) had the same reducing capacity. These data indicated that the reductive metabolism of RAB in liver subcellular fractions was not mediated by liver reductases.

Further studies were conducted to confirm the dominant components that were involved in the reductive metabolism of PPIs. As shown in Fig. 3, a concentration-dependent inhibition of reductive metabolism was observed when sulfhydryl-blocking agents (NEM, EA, and MD) were added to the HLC incubations. The amount of produced thioether was reduced to 64.9%, 52.3%, and 63.7% respectively at 100 μM of sulfhydryl-blocking agents. With further increasing concentrations of three inhibitors, the reductive metabolism was nearly completely inhibited.

Reductive reaction of RAB in GSH and cysteine solutions. RAB thioether was

detected after the incubation of RAB in GSH and cysteine solutions for 1 h. It was formed in a GSH or cysteine concentration-dependent manner (Fig. 4) when the concentration of GSH or cysteine was less than 10-fold of the substrate. However, the formation did not continue to increase when the GSH or cysteine concentration was increased to normal intracellular levels (1 mM). In addition, there is no significant difference in the rate of reduction of RAB in PBS and KPi solutions containing GSH or cysteine.

The formation rates of thioether metabolites of the four PPIs were measured in GSH solution and HLCs. As shown in Fig 5, the formation of all four thioethers in both incubation systems was time dependent within 60 minutes and the formation rate of the four PPI-thioethers differed. In both incubation systems, the formation rate of RAB was the fastest. The rank order of reduction rates in GSH was RAB > OME > LAN > PAN (Table 3). In the incubation of RAB with GSH, the two GSH conjugates identified as benzimidazole-GSH conjugate and [RAB-H2O]-GSH conjugate were observed in a GSH concentration-dependent manner (Supplemental Fig. 2).

Reductive metabolism and chiral inversion in rat liver S9 fractions. The main metabolic profiles of (*R*)-RAB in rat liver S9 incubations are shown in Fig. 6. (*R*)-RAB, (*S*)-RAB, and RAB thioether were confirmed using reference standards. The results showed that (*R*)-RAB can be converted to thioether regardless of whether GSH was added in Rat liver S9. The formation rate of RAB thioether is similar with that in other liver subcellular fractions. In the incubation of (*R*)-RAB with NADPH-supplemented rat S9, chiral inversion metabolite (*S*)-RAB and other thioether-related metabolites such as desmethyl thioether and thioether carboxylic acid were observed.

Effect of the inhibition of CYP enzyme on the reductive metabolism and chiral inversion. The average concentration versus time profiles of (*R*)-RAB, (*S*)-RAB, and

RAB thioether after intravenous administration of (*R*)-RAB are shown in Fig. 7. The noncompartmental pharmacokinetic parameters of (*R*)-RAB, (*S*)-RAB, and RAB thioether are shown in Table 4. In ABT group, the AUC of (*R*)-RAB was 4.6 times higher than that of the control group, and the AUCs of reductive metabolite and chiral inversion product in ABT group were 12.0 and 14.7 higher than those of control group, respectively. The AUC_{0-t} ratio of RAB thioether to RAB was 22.3%; however, only 8.6% was found in control group.

Discussion

PPIs show varied extent of chiral inversion in vivo. Under most circumstances, the chiral inversion degree of PPIs is small or even negligible (Andersson et al., 2001; Xie et al., 2004; Gao et al., 2013). However, obvious chiral inversion caught our attention in the phase I clinical trial of (*R*)-anaprazole, a novel PPI whose chemical properties and metabolic profiles are similar to RAB.

Thioether drugs such as cimetidine, sulindac thioether, and flosequinan thioether could all be oxidized to sulfoxide form by flavin monooxygenase or CYP enzymes (Mitchell et al., 1982; Kashiyama et al., 1997; Hamman et al., 2000). In our research, all of the four PPI-thioethers could be stereoselectively oxidized to (*R*)- and (*S*)-PPIs after incubation in HLMs. After the intravenous administration of RAB thioether, (*R*)- and (*S*)-RAB were both detected in rat plasma. Based on the in vivo and in vitro results, thioether metabolites of PPIs may be the intermediate of chiral inversion of PPIs.

Xenobiotics containing a sulfoxide moiety such as sulindac and fenthion sulfoxide could be reduced by several reductases, including aldehyde oxidase and methionine sulfoxide reductase, in the liver (Tatsumi et al., 1982; Tarrago et al., 2018). The sulfoxide reduction of flosequinan is mediated by intestinal bacteria in the small intestine (Kashiyama et al., 1994). Reductive metabolism to form thioether is also a

common metabolic pathway of PPIs; however, the main organ and the main reductases of the reductive metabolism have not been reported (Fuhr and Jetter, 2002; Pu et al., 2018). By injection via the portal vein, drugs could enter into the systemic circulation without undergoing first pass metabolism in the intestine (Kunta et al., 2004; Shin et al., 2014). Rats were administered with (*R*)-RAB via different routes. The molar AUC_{0-t} ratios of thioether to RAB in the portal vein was significantly lower than that in the systemic circulation after oral administration. The AUC_{0-t} ratio in rats administered via portal vein was also higher than that of intravenous group, respectively. These data indicated that RAB thioether was mainly formed in the liver instead of the intestine.

RAB could be chemically transformed into thioether spontaneously in PBS, while a higher reaction rate in liver subcellular fractions was observed, indicating that reductases or reducing agents were involved in the reductive pathway of PPIs. However, NADPH and NADH were not essential in the reductive process, and even the heat-deactivated HLCs also possessed the same reductive capacity as normal HLCs. The reduction rate in the extract of freshly prepared rat liver homogenates by acetonitrile was higher than that in PBS. These results proved that RAB was converted into RAB thioether mainly via non-enzymatic metabolism, and some biological reducing agents might be involved in the reductive metabolism of PPIs. Sulfhydryl-blocking agents, NEM, MD, and EA, could inhibit the reductive metabolism of RAB in liver subcellular fractions in a concentration-dependent manner. Moreover, α-β-unsaturated ketones/amides were contained in these compounds. Michael addition products between these compounds and GSH were detected in “inhibitor”-treated HLCs (Supplemental Fig. 3), suggesting that the inhibition of reduction reaction may be caused by the depletion of the thiols in liver subcellular fractions.

In addition to GSH, other thiol compounds such as cysteine and dithiothreitol

could accelerate the reduction rate of PPIs in PBS to the same degree as HLCs. Thiol depletors such as iodoacetamide could also inhibit the reductive metabolism of PPIs in HLCs (data not shown). These results revealed that the reductive metabolism of PPIs in vivo and in subcellular fractions was mediated by the endogenous biological reducing agents such as GSH and cysteine.

A marked difference exists between the in vivo concentrations of GSH and PPIs. The C_{max} of PPIs in human plasma after oral administration of OME (20 mg or 40 mg), LAN (30 mg), PAN (40 mg), and RAB (20 mg) was only approximately 0.534–9.28 μM (Huber et al., 1995; Andersson et al., 2001; Miura et al., 2005; Dash et al., 2018). However, the physiological concentrations of GSH in hepatocytes could reach 10 mM, and the levels of other endogenous thiol compounds were also significantly higher than those of PPIs (Lorincz and Szarka, 2017; Zarka and Bridge, 2017). The present study showed that when the concentration of GSH increased to more than 10 times that of PPIs, the formation rate of thioethers would no longer increase. Therefore, as long as PPIs enter the liver, they would be transformed into thioethers at a constant and maximum rate, and the reductive metabolism of PPIs could not be influenced by the physiological fluctuation of GSH concentrations. Though moderate levels of GSH were observed in the whole blood (Zarka and Bridge, 2017), PPIs could not be reduced to thioether in fresh rat and human whole blood probably because of the high degree of binding with plasma protein.

The degree of chiral inversion was directly affected by the degree of reductive metabolism of PPIs. The formation rate of RAB thioether in GSH solutions and HLCs was significantly higher than that of other PPIs. The plasma exposure of RAB thioether in humans accounted for approximately 50% of the parent drugs (Shirai et al., 2001; Miura et al., 2006), but the plasma concentrations of OME thioether and LAN thioether

were low, which could explain why the chiral inversion of OME and LAN in humans could be negligible. Meanwhile, a positive correlation was found between the natural bond orbital (NBO) charges (Reed et al., 1985; Reed et al., 1988) of sulfur atoms in these compounds and the reaction rate (Cheshmedzhieva et al., 2009) in GSH (Supplemental Table 1). The change of substituents would affect the oxidation–reduction properties of PPIs and their elimination pathways in vivo.

PPIs were eliminated from the circulation by extensive metabolism (Horn, 2004). Oxidative metabolism was the main clearance pathway for OME, LAN, and PAN, whereas reductive metabolism was the minor pathway for them. However, a new class of PPIs, including RAB and ilaprazole, was mainly metabolized via reduction to thioether (Dash et al., 2018; Pu et al., 2018). A mass balance study showed that after oral dosing of [^{14}C] RAB, the main radioactive components were thioether carboxylic acid and mercapturic acid conjugate metabolites in urine and thioether carboxylic acid in the feces, suggesting that oxidative metabolism was also needed for the final clearance of RAB. The plasma exposure of RAB thioether in humans was influenced by the activity of oxidative enzymes (Uno et al., 2006). In poor metabolizers of CYP2C19, the mean AUC values of RAB thioether were found to be 2.68 times higher than those in extensive metabolizers (Miura et al., 2005). Therefore, we evaluated the influence of CYP activities on the degree of reductive metabolism and chiral inversion of PPIs. After the inhibition of CYPs by ABT in SD rats, the AUCs of RAB thioether and chiral inversion product were both markedly increased. On the one hand, further metabolism of thioether to form thioether carboxylic acid was inhibited; on the other hand, the direct oxidative metabolism of (*R*)-RAB was also blocked. Therefore, more RAB were reduced to thioether as a compensation. Chemical inhibition or activity reduction of oxidative enzymes would increase the plasma exposure of RAB thioether

and then the degree of chiral inversion.

The mechanism of chiral inversion of PPIs in vivo was elucidated in our study. PPIs were metabolized to thioethers in the liver by biological reducing agents such as GSH and cysteine, and then thioether metabolites were stereoselectively oxidized to (*R*)- and (*S*)-PPIs to cause chiral inversion. The study is instructive for the development of single enantiomer PPIs and avoiding drug-drug interactions in clinical use due to increased plasma exposure of thioether metabolites.

DMD Fast Forward. Published on April 8, 2019 as DOI: 10.1124/dmd.118.086090
This article has not been copyedited and formatted. The final version may differ from this version.

Acknowledgements

We greatly appreciate Aosaikang Pharmaceutical (Jiangsu, China) for providing (*R*)- and (*S*)-rabeprazole.

Authorship Contributions

Participated in research design: Tang, X. Chen.

Conducted experiments: Tang, Z. Chen.

Contributed new reagents or analytic tools: Tang, Zhu, Zhong, X. Chen.

Performed data analysis: Tang, Z. Chen, Zhu, X. Chen.

Wrote or contributed to the writing of the manuscript: Tang, X. Chen.

Conflicts of interest

The authors declare no conflicts of interest.

References

Agranat I, Caner H, and Caldwell J (2002) Putting chirality to work: the strategy of chiral switches. *Nat Rev Drug Discov* **1:**753-768.

Andersson T, Hassan-Alin M, Hasselgren G, Rohss K, and Weidolf L (2001) Pharmacokinetic studies with esomeprazole, the (S)-isomer of omeprazole. *Clin Pharmacokinet* **40:**411-426.

Bourland JA, Martin DK, and Mayersohn M (1998) In vitro transesterification of cocaethylene (ethylcocaine) in the presence of ethanol. esterase-mediated ethyl ester exchange esterase-mediated ethyl ester exchange. *Drug Metab Dispos* **26:**203-206.

Cheshmedzhieva D, Ilieva S, Hadjieva B, Trayanova T, and Galabov B (2009) Reactivity of acetanilides in the alkaline hydrolysis reaction: theory vs. experiment. *Mol Phys* **107:**1187-1192.

Dash RP, Rais R, and Srinivas NR (2018) Stereoselective and nonstereoselective pharmacokinetics of rabeprazole - an overview. *Xenobiotica* **48:**422-432.

Esterbauer H, Zollner H, and Lang J (1985) Metabolism of the Lipid-Peroxidation Product 4-Hydroxynonenal by Isolated Hepatocytes and by Liver Cytosolic Fractions. *Biochem J* **228:**363-373.

Freedberg DE, Kim LS, and Yang YX (2017) The Risks and Benefits of Long-term Use of Proton Pump Inhibitors: Expert Review and Best Practice Advice From the American Gastroenterological Association. *Gastroenterology* **152:**706-715.

Fuhr U and Jetter A (2002) Rabeprazole: pharmacokinetics and pharmacokinetic drug interactions. *Pharmazie* **57:**595-601.

Gao YH, Xu JX, Su ZX, Song L, and Lou HX (2013) The chiral bioconversion and preclinical pharmacokinetic analysis of (R)-(+)-rabeprazole in beagle dogs by HPLC and HPLC-MS/MS. *Biomed Chromatogr* **27:**1380-1386.

Hamman MA, Haehner-Daniels BD, Wrighton SA, Rettie AE, and Hall SD (2000) Stereoselective sulfoxidation of sulindac sulfide by flavin-containing monooxygenases. Comparison of human liver and kidney microsomes and mammalian enzymes. *Biochem Pharmacol* **60:**7-17.

Horn J (2004) Review article: relationship between the metabolism and efficacy of proton pump inhibitors - focus on rabeprazole. *Aliment Pharm Therap* **20:**11-19.

Huber R, Kohl B, Sachs G, Senn-Bilfinger J, Simon WA, and Sturm E (1995) Review article: the continuing development of proton pump inhibitors with particular reference to pantoprazole.

Aliment Pharmacol Ther **9:**363-378.

Ikuta H, Kawase A, and Iwaki M (2017) Stereoselective Pharmacokinetics and Chiral Inversion of Ibuprofen in Adjuvant-induced Arthritic Rats. *Drug Metab Dispos* **45:**316-324.

Ishizaki T and Horai Y (1999) Review article: cytochrome P450 and the metabolism of proton pump inhibitors--emphasis on rabeprazole. *Aliment Pharmacol Ther* **13 Suppl 3:**27-36.

Kashiyama E, Yokoi T, Odomi M, Funae Y, Inoue K, and Kamataki T (1997) Cytochrome P450 responsible for the stereoselective S-oxidation of flosequinan in hepatic microsomes from rats and humans. *Drug Metabolism and Disposition* **25:**716-724.

Kashiyama E, Yokoi T, Todaka T, Odomi M, and Kamataki T (1994) Chiral inversion of drug: role of intestinal bacteria in the stereoselective sulphoxide reduction of flosequinan. *Biochem Pharmacol* **48:**237-243.

Kunta JR, Lee SH, Perry BA, Lee YH, and Sinko PJ (2004) Differentiation of gut and hepatic first-pass loss of verapamil in intestinal and vascular access-ported (IVAP) rabbits. *Drug Metab Dispos* **32:**1293-1298.

Landes BD, Miscoria G, and Flouvat B (1992) Determination of Lansoprazole and Its Metabolites in Plasma by High-Performance Liquid-Chromatography Using a Loop Column. *J Chromatogr-Biomed* **577:**117-122.

Li XQ, Andersson TB, Ahlstrom M, and Weidolf L (2004) Comparison of inhibitory effects of the proton pump-inhibiting drugs omeprazole, esomeprazole, lansoprazole, pantoprazole, and rabeprazole on human cytochrome P450 activities. *Drug Metab Dispos* **32:**821-827.

Lorincz T and Szarka A (2017) The determination of hepatic glutathione at tissue and subcellular level. *J Pharmacol Toxicol Methods* **88:**32-39.

Marom H, Biedermann PU, and Agranat I (2007) Pyramidal inversion mechanism of simple chiral and achiral sulfoxides: a theoretical study. *Chirality* **19:**559-569.

Mitchell SC, Idle JR, and Smith RL (1982) The metabolism of [14C]cimetidine in man. *Xenobiotica* **12:**283-292.

Miura M, Tada H, Satoh S, Habuchi T, and Suzuki T (2006) Determination of rabeprazole enantiomers and their metabolites by high-performance liquid chromatography with solid-phase extraction. *J Pharmaceut Biomed* **41:**565-570.

Miura M, Tada H, Yasui-Furukori N, Uno T, Sugawara K, Tateishi T, and Suzuki T (2005)

Enantioselective disposition of lansoprazole in relation to CYP2C19 genotypes in the presence of fluvoxamine. *Br J Clin Pharmacol* **60:**61-68.

Pu J, Wang F, Tang W, and Zhu MS (2018) Biotransformation of Ilaprazole in Human Liver Microsomes and Human: Role of CYP3A4 in Ilaprazole Clearance and Drug-Drug Interaction. *Drug Metabolism and Disposition* **46:**1453-1461.

Rayner DR, Gordon AJ, and Mislow K (1968) Thermal Racemization of Diaryl Alkyl Aryl and Dialkyl Sulfoxides by Pyramidal Inversion. *J Am Chem Soc* **90:**4854-&.

Reed AE, Curtiss LA, and Weinhold F (1988) Intermolecular Interactions from a Natural Bond Orbital, Donor-Acceptor Viewpoint. *Chem Rev* **88:**899-926.

Reed AE, Weinstock RB, and Weinhold F (1985) Natural-Population Analysis. *J Chem Phys* **83:**735-746.

Reist M, Carrupt PA, Francotte E, and Testa B (1998) Chiral inversion and hydrolysis of thalidomide: Mechanisms and catalysis by bases and serum albumin, and chiral stability of teratogenic metabolites. *Chemical Research in Toxicology* **11:**1521-1528.

Rezk NL, Brown KC, and Kashuba AD (2006) A simple and sensitive bioanalytical assay for simultaneous determination of omeprazole and its three major metabolites in human blood plasma using RP-HPLC after a simple liquid-liquid extraction procedure. *J Chromatogr B Analyt Technol Biomed Life Sci* **844:**314-321.

Setoyama T, Drijfhout WJ, de Merbel NCV, Humphries TJ, and Hasegawa J (2006) Mass balance study of [C-14] rabeprazole following oral administration in healthy subjects. *Int J Clin Pharm Th* **44:**557-565.

Shin BS, Yoo SD, Kim TH, Bulitta JB, Landersdorfer CB, Shin JC, Choi JH, Weon KY, Joo SH, and Shin S (2014) Quantitative determination of absorption and first-pass metabolism of apicidin, a potent histone deacetylase inhibitor. *Drug Metab Dispos* **42:**974-982.

Shin JM and Kim N (2013) Pharmacokinetics and pharmacodynamics of the proton pump inhibitors. *J Neurogastroenterol Motil* **19:**25-35.

Shirai N, Furuta T, Moriyama Y, Okochi H, Kobayashi K, Takashima M, Xiao F, Kosuge K, Nakagawa K, Hanai H, Chiba K, Ohashi K, and Ishizaki T (2001) Effects of CYP2C19 genotypic differences in the metabolism of omeprazole and rabeprazole on intragastric pH. *Aliment Pharmacol Ther* **15:**1929-1937.

Tarrago L, Oheix E, Peterfi Z, and Gladyshev VN (2018) Monitoring of Methionine Sulfoxide Content

and Methionine Sulfoxide Reductase Activity. *Methods Mol Biol* **1661:**285-299.

Tatsumi K, Kitamura S, and Yamada H (1982) Involvement of liver aldehyde oxidase in sulfoxide reduction. *Chem Pharm Bull (Tokyo)* **30:**4585-4588.

Tomaszewski J and Rumore MM (1994) Stereoisomeric Drugs: FDA's Policy Statement and the Impact on Drug Development. *Drug Dev Ind Pharm* **20:**119-139.

Uno T, Shimizu M, Yasui-Furukori N, Sugawara K, and Tateishi T (2006) Different effects of fluvoxamine on rabeprazole pharmacokinetics in relation to CYP2C19 genotype status. *Brit J Clin Pharmaco* **61:**309-314.

Uno T, Yasui-Furukori N, Shimizu M, Sugawara K, and Tateishi T (2005) Determination of rabeprazole and its active metabolite, rabeprazole thioether in human plasma by column-switching high-performance liquid chromatography and its application to pharmacokinetic study. *J Chromatogr B Analyt Technol Biomed Life Sci* **824:**238-243.

Williams RC, Riley CM, Sigvardson KW, Fortunak J, Ma P, Nicolas EC, Unger SE, Krahn DF, and Bremner SL (1998) Pharmaceutical development and specification of stereoisomers. *J Pharm Biomed Anal* **17:**917-924.

Xie ZY, Yang BH, Zhang YF, and Zhong DF (2004) Studies on chiral inversion of dextropantoprazole in human. *Yao Xue Xue Bao* **39:**370-373.

Zarka MH and Bridge WJ (2017) Oral administration of gamma-glutamylcysteine increases intracellular glutathione levels above homeostasis in a randomised human trial pilot study. *Redox Biol* **11:**631-636.

Zhou Q, Yan XF, Pan WS, and Zeng S (2008) Is the required therapeutic effect always achieved by racemic switch of proton-pump inhibitors? *World J Gastroentero* **14:**2617-2619.

Footnotes

This research was financially supported by the National Natural Science Foundation of China [81573500] and the Strategic Priority Research Program of the Chinese Academy of Sciences [XDA 12050306].

Figure legends

Fig. 1. Average plasma concentration of RAB thioether, (*R*)-RAB, and (*S*)-RAB versus time curves after the intravenous administration of RAB thioether (1 mg/kg) in SD rats. Data are presented as the mean ± S.D. (n = 5).

Fig. 2. Amount of formed RAB thioether after the incubation of RAB (1.5 μM) in different liver subcellular fractions. Results are expressed as the mean ± S.D. (n = 3).

Fig. 3. Amount of formed RAB thioether after the incubation of RAB (1.5 μM) in HLCs treated with different concentrations of NEM, EA, and MD. Results are expressed as the mean ± S.D. (n = 3).

Fig. 4. Amount of formed RAB thioether after the incubation of racemic RAB (1.5 μM) with different concentrations of GSH and cysteine in PBS and KPi solutions. Results are expressed as the mean ± S.D. (n = 3).

Fig. 5. Formation of thioether metabolites after the incubation of four racemic PPIs (1.5 μM) in GSH solution (1000 μM) (A) and HLCs (B). Results are expressed as the mean ± S.D. (n = 3).

Fig. 6. MS detection of the main metabolic profiles of (*R*)-RAB in rat liver S9: in the absence of both NADPH and GSH (A), in the presence of GSH but not NADPH (B), in the presence of GSH but not NADPH (C). in the presence of both NADPH and GSH (D), The chromatogram of mixture solution of racemic RAB (50 nM) and RAB thioether (10 nM) was provided (E).

Fig. 7. Mean plasma concentration–time profiles of (*R*)-RAB (A), RAB thioether (B), and (*S*)-RAB (C) on the ABT-treated (100 mg/kg) rats and control rats after intravenous doses of (*R*)-RAB (3 mg/kg). Data are presented as the mean ± S.D. (n = 4).

Fig. 8. Proposed mechanism of chiral inversion of PPIs and structure of commonly used proton-pump inhibitors. The general structure of PPIs are given. and the R represents different substituent groups (numbers represent different substituents).

Table 1.

Kinetic parameters for the formation of (*R*)- and (*S*)-PPIs from PPI-thioethers in HLMs. Values are means ± S.D., *n* = 3.

Parameters	OME		LAN		PAN		RAB	
	R	*S*	*R*	*S*	*R*	*S*	*R*	*S*
V_{max} (nmol/min/mg protein)	1.1 ± 0.0	0.95 ± 0.03	0.12 ± 0.01	0.032 ± 0.002	0.051 ±0.002	0.16 ± 0.01	0.27 ± 0.01	0.18 ± 0.01
K_m (μM)	36 ± 3	74 ± 6	77 ± 14	78 ± 13	6.1 ±1.2	11 ± 1.8	18 ± 1	72 ± 4
V_{max}/K_m (μL/min/mg protein)	31 ± 2	13 ± 1	1.7 ± 0.2	0.41 ± 0.04	8.4 ± 1.4	15 ± 2	15 ± 1	2.5 ± 0.1

DMD Fast Forward. Published on April 8, 2019 as DOI: 10.1124/dmd.118.086090
This article has not been copyedited and formatted. The final version may differ from this version.

Table 2.

The area under the plasma concentration–time curve (AUC) of RAB thioether and (*R*)-RAB after three administration routes (oral administration (*n*=5) in portal vein- cannulated rats, portal vein administration (*n*=4) and intravenous administration (*n*=4) in normal SD rats) of 3 mg/kg of (*R*)-RAB. Results are expressed as the mean ± S.D.

Administration route	$AUC_{0\text{-}t}$ of thioether (ng·h/mL)	$AUC_{0\text{-}t}$ of (*R*)-RAB (ng·h/ mL)	AUC ratio[c]
oral[a]	3.75 ± 1.09	12.8 ± 5.3	30.6%
oral[b]	15.5 ± 3.0	137 ± 64	11.8%
portal vein	25.0 ± 3.38	91.3 ± 34.2	28.6%
intravenous	73.9 ± 8.75	500 ± 46.7	15.5%

a: from systemic plasma concentration in circulation; b: from portal vein plasma concentration; c: $M_{RAB} \times AUC_{0\text{-t thioether}} / M_{thioether} \times AUC_{0\text{-t RAB}}$, M represents the average molecular weight.

DMD Fast Forward. Published on April 8, 2019 as DOI: 10.1124/dmd.118.086090
This article has not been copyedited and formatted. The final version may differ from this version.

Table 3.

Formation rate (nmol/L/min) of PPI-thioethers in GSH and HLCs. Results are expressed as the mean ± S.D. (*n* = 3).

Incubation system	PAN	LAN	OME	RAB
GSH	0.281 ± 0.025	0.460 ± 0.094	0.573 ± 0.028	4.33 ± 0.37
HLCs	0.218 ± 0.019	0.354 ± 0.012	0.377 ±0.016	3.78 ± 0.02

DMD Fast Forward. Published on April 8, 2019 as DOI: 10.1124/dmd.118.086090
This article has not been copyedited and formatted. The final version may differ from this version.

Table 4.

Pharmacokinetic parameters of (*R*)-RAB, (*S*)-RAB, and RAB thioether obtained after the intravenous injection of (*R*)-RAB (3 mg/kg) in ABT-treated rats and control rats. Results are expressed as the mean ± S.D. (*n* = 4).

Component		AUC_{0-t} (ng·h/ mL)	$AUC_{0-\infty}$ (ng·h/ mL)	$t_{1/2}$ (h)	MRT (h)
(*R*)-RAB	ABT	2858 ± 325	2891 ± 354	0.273 ± 0.052	0.360 ± 0.008
	Control	621 ± 72	621 ± 73	0.122 ± 0.009	0.165 ± 0.007
Thioether	ABT	609 ± 146	610 ± 147	1.02 ± 0.08	1.55 ± 0.13
	Control	50.8 ± 2.8	50.9 ± 2.8	1.01 ± 0.11	0.656 ± 0.043
(*S*)-RAB	ABT	4.57 ± 1.10	-	0.913 ± 0.070	1.19 ± 0.08
	Control	0.31 ± 0.08	-	-	0.159 ± 0.015

The em dash symbols indicate no value because of the lack of time points to calculate.

DMD Fast Forward. Published on April 8, 2019 as DOI: 10.1124/dmd.118.086090
This article has not been copyedited and formatted. The final version may differ from this version.

Fig. 1.

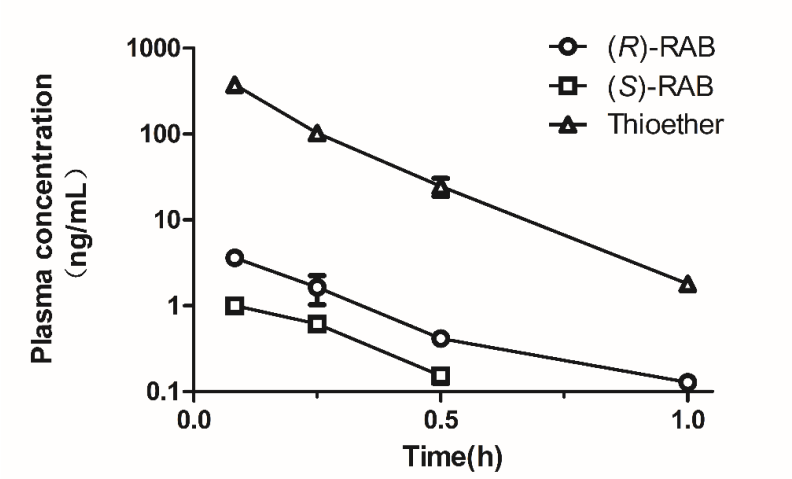

DMD Fast Forward. Published on April 8, 2019 as DOI: 10.1124/dmd.118.086090
This article has not been copyedited and formatted. The final version may differ from this version.

Fig. 2.

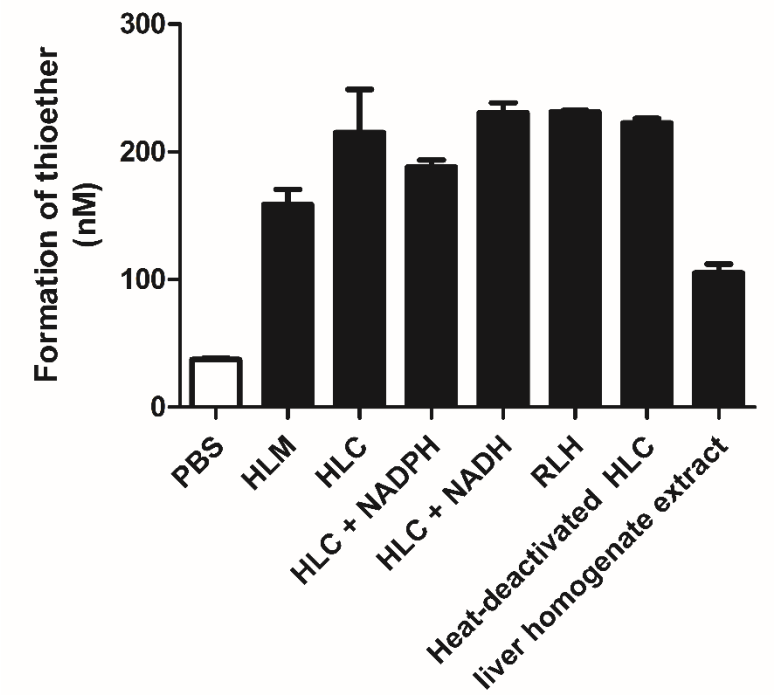

DMD Fast Forward. Published on April 8, 2019 as DOI: 10.1124/dmd.118.086090
This article has not been copyedited and formatted. The final version may differ from this version.

Fig. 3.

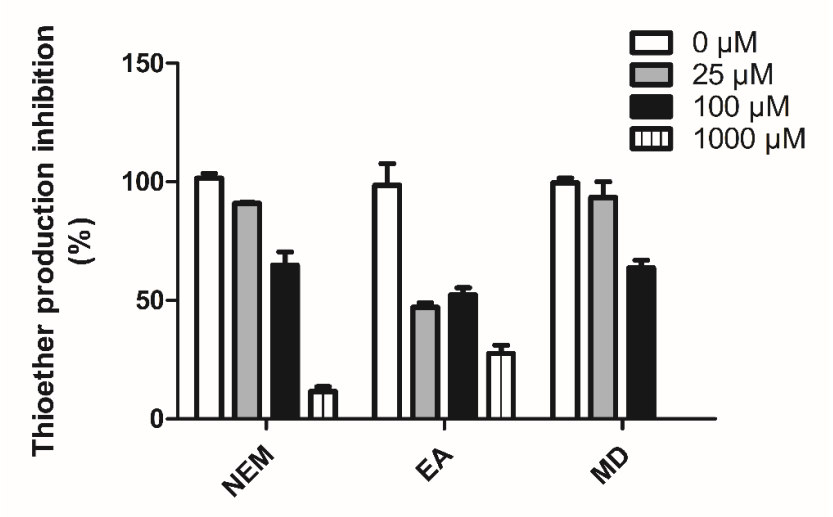

DMD Fast Forward. Published on April 8, 2019 as DOI: 10.1124/dmd.118.086090
This article has not been copyedited and formatted. The final version may differ from this version.

Fig. 4.

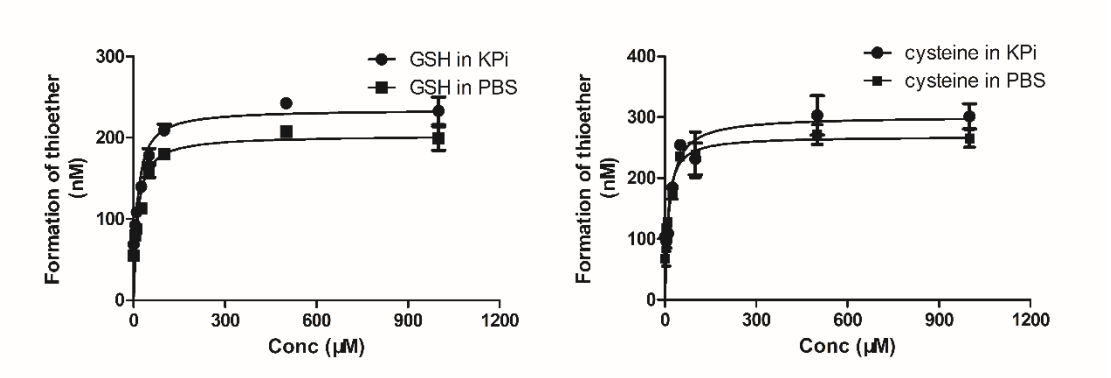

Fig. 5.

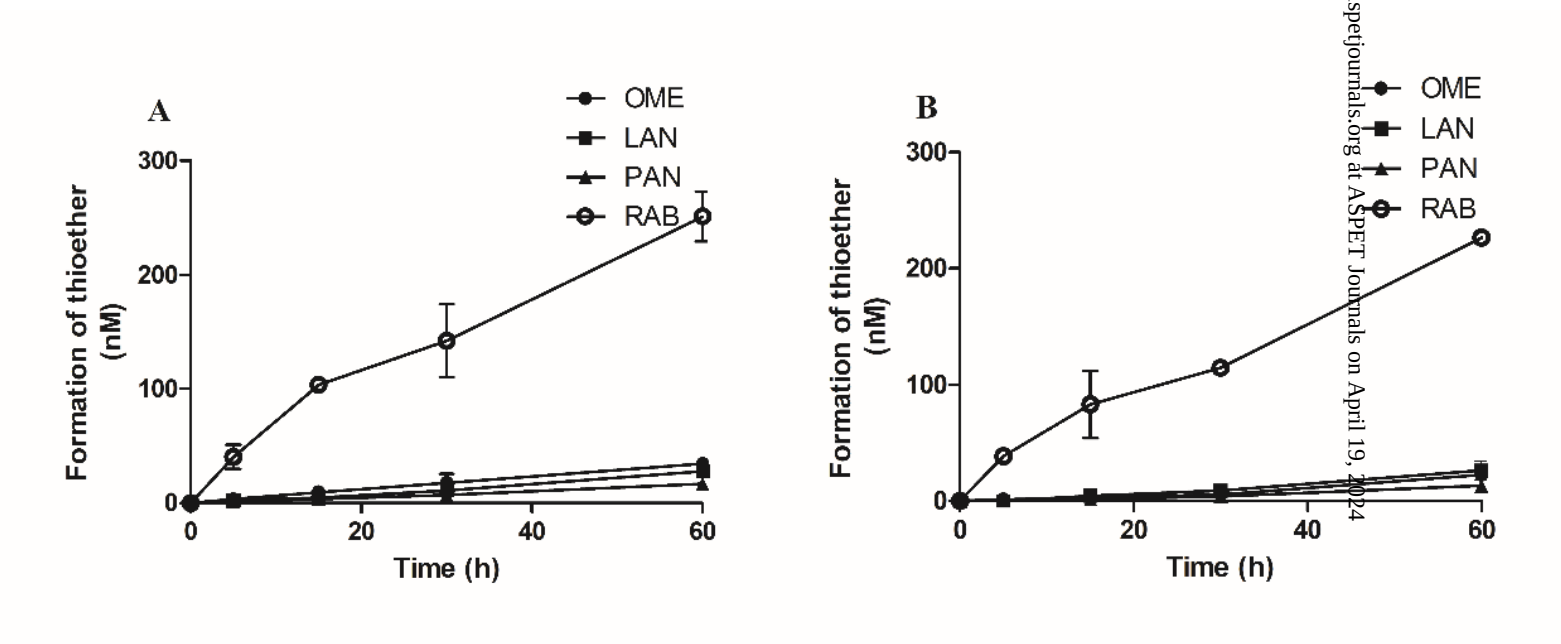

Fig. 6.

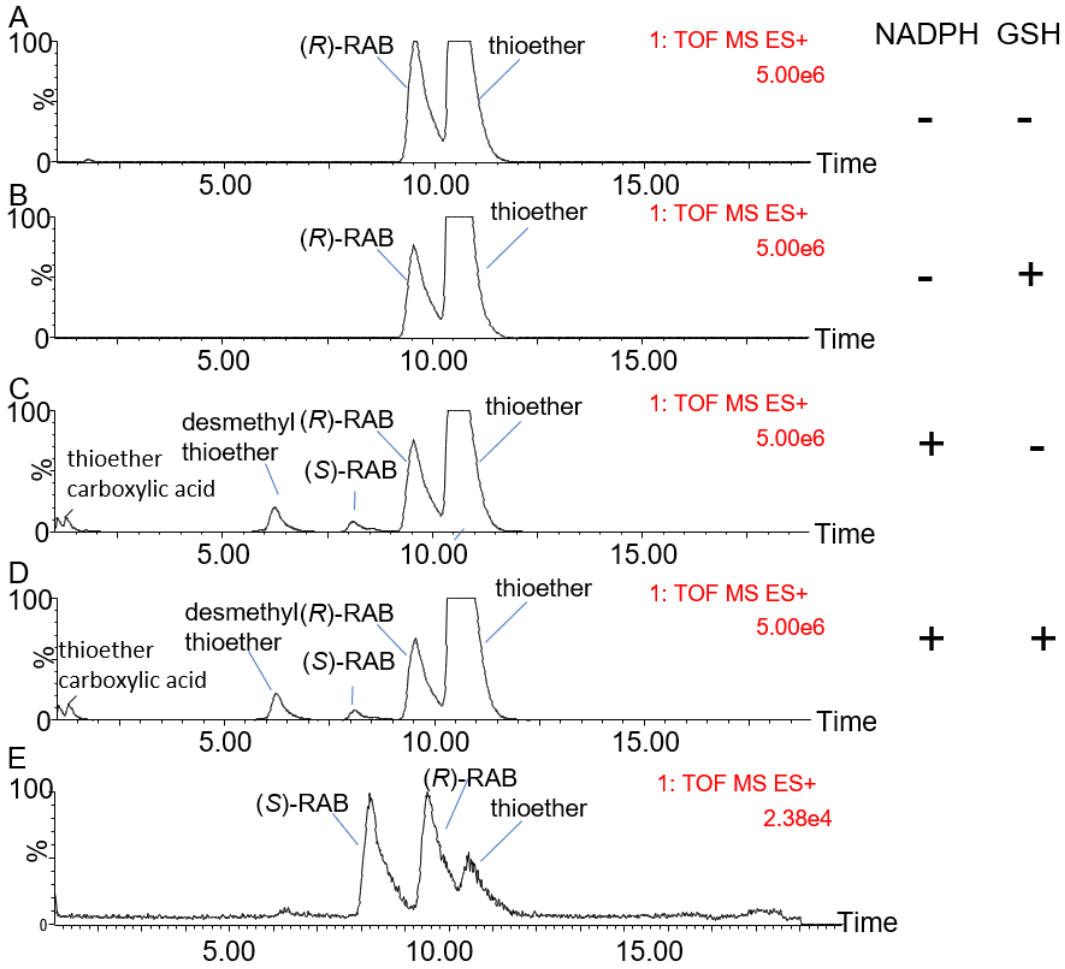

Fig. 7.

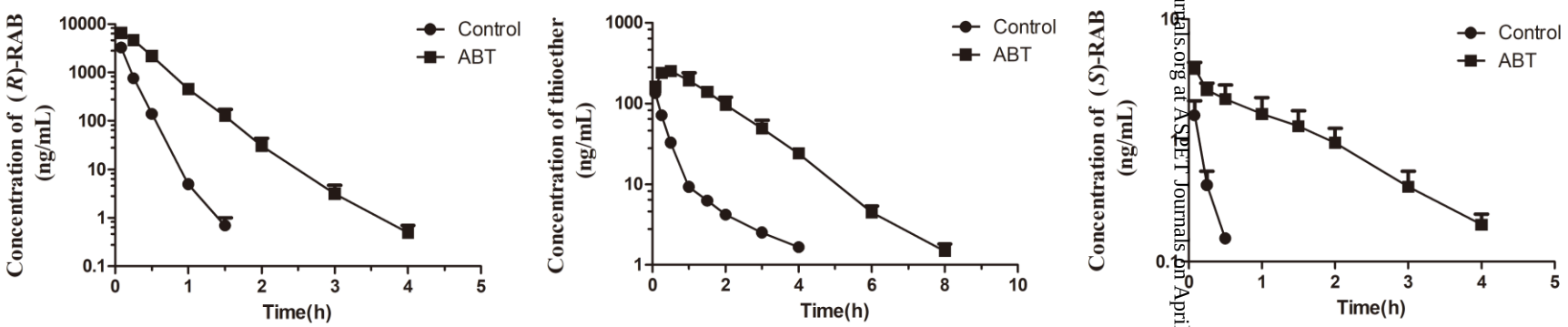

Fig. 8.

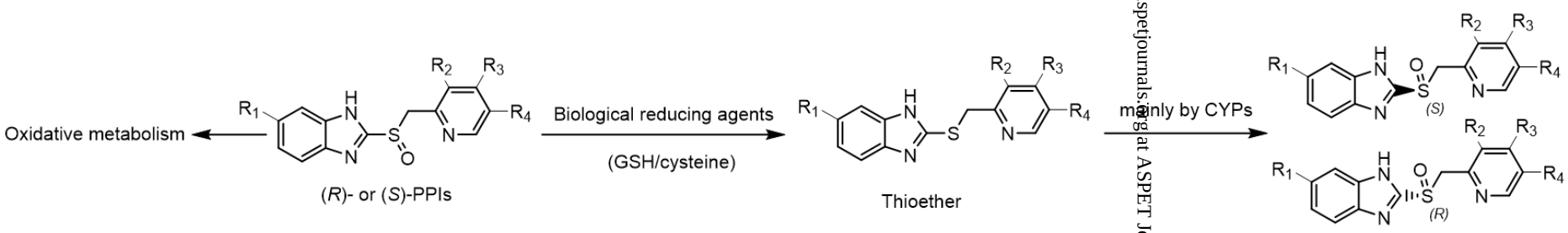

Substituents	OME	PAN	LAN	RAB
R_1	$-OCH_3$	$-OCHF_2$	-H	-H
R_2	$-CH_3$	$-OCH_3$	$-CH_3$	$-CH_3$
R_3	$-OCH_3$	$-OCH_3$	$-OCH_2CF_3$	$-OCH_2CH_2CH_2OCH_3$
R_4	$-CH_3$	-H	-H	-H

SUPPLEMENTARY

Mechanism of Reductive Metabolism and Chiral Inversion of Proton Pump Inhibitors

Chongzhuang Tang[a,b], Zhaoqiang Chen[a], Xiaojian Dai[a], Weiliang Zhu[a,b], Dafang Zhong[a,b], Xiaoyan Chen[a,b]

[a] Shanghai Institute of Materia Medica, Chinese Academy of Sciences, 501 Haike Road, Shanghai 201203, P.R. China

[b] University of Chinese Academy of Sciences, No.19A Yuquan Road, Beijing 100049, China

Drug Metabolism and Disposition

Formation of PPIs from PPI-thioethers in FMOs. (*R*)- and (*S*)-PPIs were also detected in thioether-fortified incubated samples with FMO1, FMO3, and FMO5, but the yields were significantly lower than those in HLM incubations (Supplemental Fig. 1). And the formation in FMO-deactivated liver microsomes (by heating) showed no difference with that in the untreated liver microsomes.

Characterization of GSH conjugates by Q-TOF MS. In the incubation of RAB with GSH, the two GSH conjugates were detected by UPLC-Q-TOF. Based on the accurate molecular weight and related fragmentation information, the components were speculated as benzimidazole-GSH conjugate and [RAB-H2O]-GSH conjugate. The detailed information including chromatograms, low collision energy mass spectra, and MS2 mass spectra are provided in supplemental materials (Supplemental Fig. 2).

To prove that the inhibition of reductive metabolism in liver subcellular fractions by NEM, EA, and MD was caused by the depletion of thiols, GSH conjugates of each inhibitor were detected by a Waters Synapt Q-TOF system. In positive ion mode, the singly charged $[M+H]^+$ ions at *m*/*z* 433.137 (NEM-GSH), 610.103 (EA-GSH), and 478.216 (MD-GSH) were observed in a low collision energy spectrum. The MS/MS spectrum showed the indicative characteristic fragment ions associated with the

cleavage of the GSH moiety (Supplemental Fig. 3-C, F, and I).

The product ions at *m*/*z* 358.106 and 304.095 were derived from the neutral loss of glycine portion (75.032 Da) and pyroglutamic acid portion (129.043 Da) and from NEM-GSH conjugate's parent ion *m*/*z* 433.137, respectively (Supplemental Fig. 3-C). The cleavage of the cysteinyl C-S bond of the GSH moiety attributes to the formation of *m*/*z* 158.028. The fragmentation pathway of the EA-GSH conjugate was similar to that of the NEM-GSH conjugate (Supplemental Fig. 3-F). The conjugate of MD and GSH underwent a two-electron oxidation, so its $[M+H]^+$ was *m*/*z* 478.126. The high-abundance product ion *m*/*z* 331.074 was formed by the neutral loss of glycine and water (Supplemental Fig. 3-I). These results confirmed the hypothesis that NEM, EA, and MD inhibit the transformation of PPIs to PPI-thioethers through the depletion of the PPI-thioethers biological reducing agents such as reduced GSH and cysteine.

DFT calculations and NBO analysis. The structures of four PPIs (OME, PAN, LAN, and RAB) were optimized by the M06-2X method at the 6-31g(d) level basis set. To confirm that the optimized conformation is indeed a minimum on the potential energy surface, normal-mode vibrational frequencies were calculated at the same level. NBO charge populations demonstrated the optimized conformations. All of these calculations were performed using the Gaussian 09 suite program.

The detailed NBO charge population is shown in Supplemental Table 1, which indicates a positive correlation between the NBO charges of sulfur atoms in these compounds and the reaction rate.

Supplemental Fig. 1. Formation of (*R*)- and (*S*)-PPIs after incubations of PPI thioethers (3 μM) in HLM (1 mg/mL) and 1 mg/mL three isoforms of recombinant FMOs (FMO1, FMO3 and FMO5). (A): (*R*)-OME. (B): (*R*)-PAN. (C): (*R*)-LAN. (D): (*R*)-RAB. (E): (*S*)-OME. (F): (*S*)-PAN. (G): (*S*)-LAN (H): (*S*)-RAB

Supplemental Fig. 2. Extracted ion chromatogram (EIC) of benzimidazole-GSH conjugate and [RAB-H2O]-GSH conjugate in the incubations of GSH solution (1 mM) and RAB in positive mode with the following MS^2 spectra. (A) EIC of benzimidazole-GSH (*m*/z 424.13). (B) low collision energy mass spectra of benzimidazole-GSH (*m*/*z* 424.13). (C) MS^2 mass spectra of benzimidazole-GSH (*m*/*z* 424.13). (D) EIC of [RAB-H2O]-GSH (*m*/*z* 649.21). (E) low collision energy mass spectra of [RAB-H2O]-GSH (*m*/*z* 649.21). (F) MS^2 mass spectra of [RAB-H2O]-GSH (*m*/*z* 649.21).

Supplemental Fig. 3. Extracted ion chromatogram (EIC) of NEM-GSH, EA-GSH, and MD-GSH conjugates in HLCs (1 mg/mL of protein) and GSH solution (1 mM) incubations in positive mode with the following MS^2 spectra. (A) EIC of NEM-GSH (*m*/*z* 433.14) in NEM-treated HLCs. (B) EIC of NEM-GSH (*m*/*z* 433.14) in NEM-treated GSH solutions. (C) MS^2 spectra of NEM-GSH (*m*/*z* 433.14) in NEM-treated GSH solutions. (D) EIC of EA-GSH (*m*/*z* 610.10) in EA-treated HLCs. (E) EIC of EA-GSH (*m*/*z* 610.10) in EA-treated GSH solutions. (F) MS^2 spectra of EA-GSH (*m*/*z* 610.10) in EA-treated GSH solutions. (G) EIC of MD-GSH (*m*/*z* 478.13) in MD-treated HLCs. (H) EIC of MD-GSH (*m*/*z* 478.13) in MD-treated GSH solutions. (I) MS^2 spectra of MD-GSH (*m*/*z* 478.13) in MD-treated GSH solutions.

Supplemental Table 1.

The selected NBO charge of important atoms in four PPIs[a].

Atom	PAN	LAN	OME	RAB
q(S)	1.317	1.319	1.326	1.339
q(O)	-1.004	-0.994	-0.989	-0.998

[a]All charges are given in au.

Supplemental Fig. 1

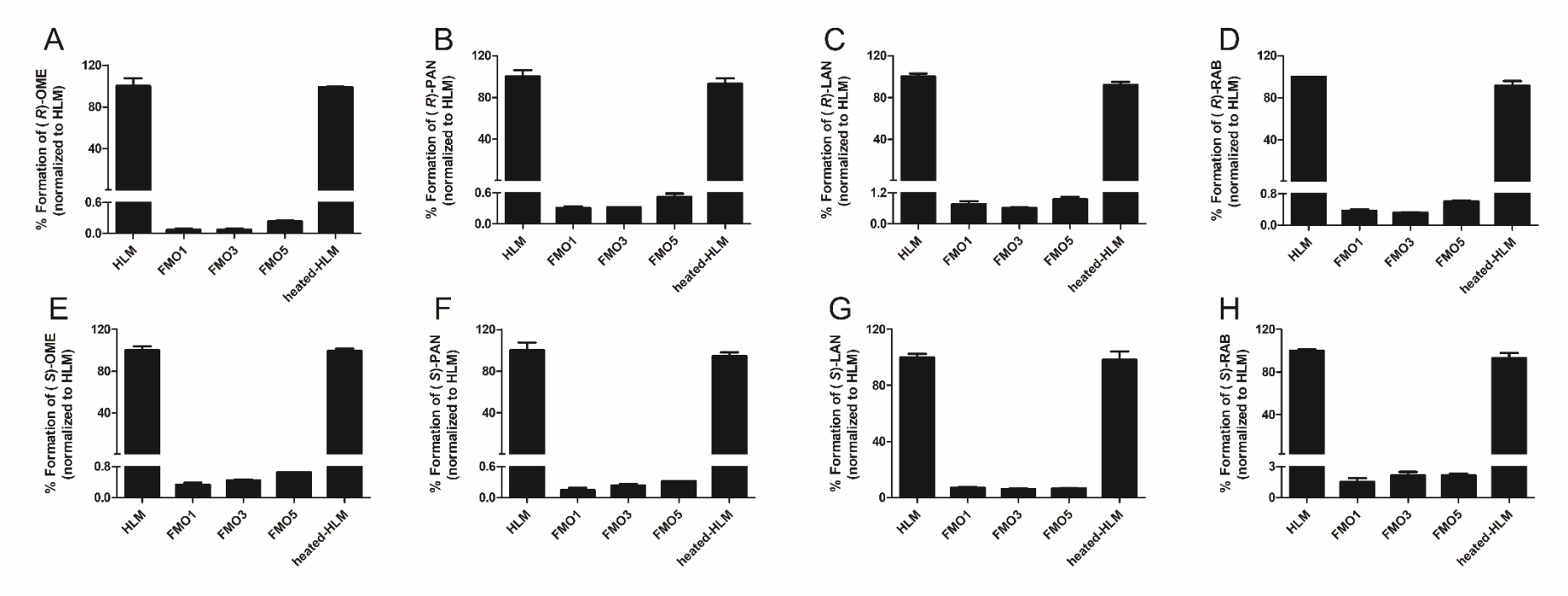

Supplemental Fig. 2

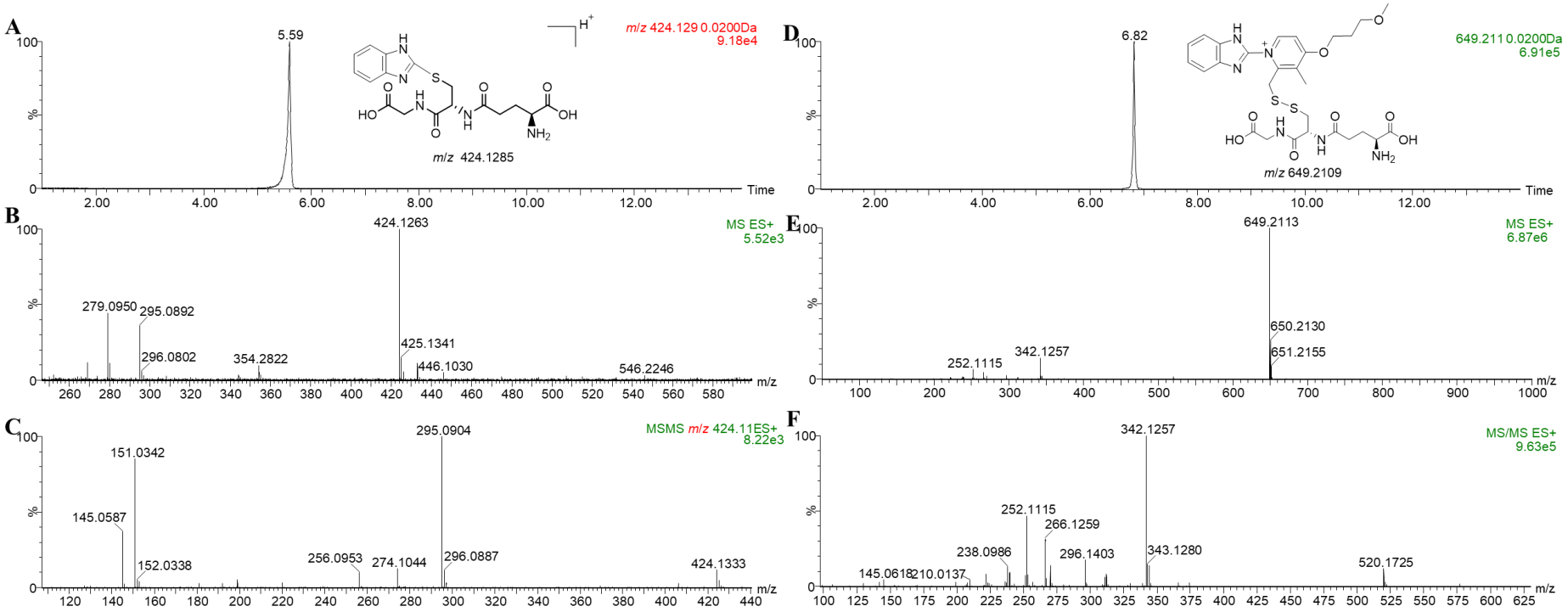

Supplemental Fig. 3